# Carbon Dioxide and Hydrogen Sulfide Removal from Simulated Landfill Gas Using Steel Slag

Jyoti K. Chetri

Graduate Research Assistant, University of Illinois at Chicago, Department of Civil, Materials, and Environmental Engineering, 842 West Taylor Street, Chicago, IL 60607, USA, e-mail: jkc4@uic.edu

Krishna R. Reddy*

Professor, University of Illinois at Chicago, Department of Civil, Materials, and Environmental Engineering, 842 West Taylor Street, Chicago, IL 60607, USA, e-mail: kreddy@uic.edu

(*Corresponding author)

Dennis G. Grubb

President, Fugacity LLC, 126 Veronica Lane, Lansdale, PA 19446, USA;

e-mail: dggrubbphdpe@gmail.com

Manuscript Submitted to:

*Journal of Environmental Engineering, ASCE*

July 25, 2020

**Abstract**

Municipal solid waste landfills are a source of major greenhouse gases such as methane ($CH_4$) and carbon dioxide ($CO_2$) while also emit trace amount of hydrogen sulfide ($H_2S$). Recently, steel slag has extensively been used for mineral $CO_2$ sequestration to minimize the $CO_2$ releases to the atmosphere. This study explores the potential of basic oxygen furnace slag (BOF) steel slag to simultaneously remove $CO_2$ and $H_2S$ from landfill gas (LFG). Various batch and column tests were conducted to evaluate the $CO_2$ and $H_2S$ removal potential of the BOF slag under various conditions such as moisture content and particle size of the BOF slag. The three different particle sizes of BOF slag (coarse, as-is, and fine) were exposed to continuous flow of a synthetic LFG [50% $CO_2$, 48.25% $CH_4$ and 1.75% $H_2S$ by volume (*v/v*)] in a column reactor to evaluate the effect of particle size on $CO_2$ and $H_2S$ removal capacity of the slag. Similarly, the BOF slag was exposed to synthetic LFG as well as 20% (*v/v*) of $H_2S$ alone in batch reactors at varying moisture contents (10–30% by weight) to evaluate the effect of moisture content on the $CO_2$ and $H_2S$ removal capacity of the slag. A significant $H_2S$ removal of 27 g $H_2S$ $kg^{-1}$ BOF slag and $CO_2$ removal of 76 g $CO_2$ $kg^{-1}$ BOF slag were obtained in the batch reactor. The fine BOF slag (< 0.106 mm) showed the maximum $CO_2$ removal (300 g $CO_2$ $kg^{-1}$ BOF slag) and $H_2S$ removal (38 g $H_2S$ $kg^{-1}$ BOF slag) upon exposure to continuous synthetic LFG flow in the column reactor. The quantitative X-Ray diffraction (QXRD) analysis showed highest increase in carbon (77.5 g C $kg^{-1}$ BOF slag) and sulfur (28 g S $kg^{-1}$ BOF slag) contents in the fine BOF slag which was consistent with the mass balance of carbon and sulfur from $CO_2$ and $H_2S$ uptake in column tests. The major reaction product with $H_2S$ was elemental sulfur depicted by the significant increase in the sulfur content in the X-ray fluorescence analysis. The key minerals involved in carbonation reactions were lime, portlandite, and larnite as these minerals showed significant reduction in weight percentage (100%, 82% and

80%, respectively) in the QXRD analysis. Overall, BOF slag showed promising results in mitigating $CO_2$ and $H_2S$ from LFG.

**Keywords:** Municipal solid waste; landfill gas emissions; BOF slag; carbon dioxide removal; hydrogen sulfide removal.

## Introduction

Municipal solid waste (MSW) landfills are the third largest source of anthropogenic methane ($CH_4$) emissions in the United States and are also a major source of carbon dioxide ($CO_2$) emissions, each constituting 50% of the landfill gas (LFG) composition (USEPA, 2020), and odor problems (Ng et al. 2017; Lee et al. 2017). $CH_4$ and $CO_2$ are two of the most abundant greenhouse gases and principal contributors to the global climate change. Odor control persists as one of the key concerns for landfill operators due to the malodorous compounds such as hydrogen sulfide ($H_2S$), methyl mercaptan, and methyl sulfide (He et al. 2011). For example, LFG from MSW landfills contains 100 to 1,000 ppm $H_2S$ (Ng et al. 2017) which is a major odor causing component, even at very low concentrations [0.01 to 1.5 parts per million (ppm)] (Ko et al. 2015). $H_2S$ concentrations above 100 ppm are immediately dangerous to life and health as stated by the U.S. Occupational Safety and Health Administration and the permissible exposure limit (8-hour limit) for $H_2S$ is 10 ppm (OSHA, 2020). In addition, $H_2S$ is also highly flammable with explosive range in air at 4.5 to 45.5% by volume (*v/v*) (OSHA, 2020). Hence, $H_2S$ emissions from landfills is a serious concern.

Active landfills having waste-to-energy plants and/or $CH_4$ recovery plants use various technologies to purify LFG to usable $CH_4$ products. The LFG purification process involves removal of moisture, particulates, and gases (such $CO_2$ and $H_2S$), and volatile organic compounds such as siloxanes (Peterson 2013). Various processes to scrub $CO_2$ and $H_2S$ from LFG involve physical and chemical adsorption. Adsorption using activated carbon, zinc oxide, and iron oxide and amine scrubbing (such as Selexol) are the most common $H_2S$ removal technologies but are cost intensive (Deed et al. 2004; Spiegel et al. 1995). Similarly, adsorption on activated carbon

74 beds, silicates or molecular sieves, dissolution of $CO_2$ in the solvents forming carbonates, water
75 scrubbing, etc. are some of the popular techniques for removing $CO_2$ from LFG (Schumacher
76 1983). Although there are many technologies available to treat $H_2S$ and $CO_2$ in LFG, they are used
77 mostly during $CH_4$ recovery process to obtain high purity $CH_4$ and hence are feasible when the
78 $CH_4$ concentrations in the LFG are high (Arkharov et al. 2016). Similarly, older landfills do not
79 have gas collection systems, and even at modern engineered landfills with the gas collection
80 systems fugitive LFG emissions persist due to the limited efficiency of gas recovery systems
81 (Scheutz et al. 2009). Accordingly, alternative approaches are needed to address fugitive LFG
82 emissions migrating through landfill capping systems.

83 Steel slag, a byproduct from steel making and refining processes, are generated in huge
84 quantity every year of which nearly 60–85% are used in construction applications and the
85 remaining 15–40% are either stockpiled or landfilled (Yildrim and Prezzi 2015). Because of its
86 alkalinity, the use of steel making slag has recently been explored for mineral carbon sequestration
87 applications (Huijgen et al. 2005; Bonenfant et al. 2008; Chetri et al. 2019). Steel slag is primarily
88 composed of calcium (Ca), iron (Fe), magnesium (Mg) and silicon (Si) which exist in both
89 crystalline and amorphous phases (Caicedo-Ramirez et al. 2020; Yildrim and Prezzi 2011). Steel
90 slag has shown promising potential to sequester $CO_2$ in the previous studies (Huijgen et al. 2005;
91 Bonenfant et al. 2008; Ukwattage et al. 2017; Chetri et al. 2019). Iron oxides have been commonly
92 used in sweetening of natural gas or landfill gas (Davydov et al. 1998). Iron oxides serve as suitable
93 oxidizing agents for $H_2S$ removal (Cantrell et al. 2003; Więckowska 1995). Iron has been found
94 to be the metal of choice for the removal of $H_2S$ as $H_2S$ reduces $Fe^{3+}$ to $Fe^{2+}$ under anerobic
95 condition as shown in **Eq. 1** (Bergersen and Haarstad 2008). The ferric oxide ($Fe_2O_3$) reacts with
96 $H_2S$ to produce $Fe_2S_3$ which is thermodynamically unstable and reacts further to form pyrite ($FeS_2$)

and ferric sulfide ($Fe_3S_4$) (Davydov et al. 1998) as shown in **Eq. 2** and **3**. In addition, the ferrous oxide (FeO) can react with $H_2S$ in aqueous solution to form ferrous sulfide (FeS) as shown in **Eq. 4** (Sarperi et al. 2014; Rickard and Luther 2007). Similarly, the high alkalinity of BOF slag favors the dissociation of $H_2S$ into $HS^-$ (bisulfide) and $S^{2-}$ (sulfide) (pKa for $H_2S/HS^-$ = 7, $HS^-/S^{2-}$ > 11) which in turn react with the metal ions such as iron leading to the formation of elemental sulfur and metal sulfides (Montes Moran et al. 2012).

$$2Fe(OH)_3(s) + 3H_2S(g) \rightarrow 2FeS(s) + \frac{1}{8}S_8(s) + 6H_2O \quad (1)$$

$$Fe_2O_3(s) + 3H_2S(g) \rightarrow Fe_2S_3(s) + 3H_2O \quad (2)$$

$$2Fe_2S_3(s) \rightarrow FeS_2(s) + Fe_3S_4(s) \quad (3)$$

$$FeO\ (s) + H_2S \rightarrow FeS\ (s) + H_2O \quad (4)$$

Owing to the high iron oxide content of the steel slags, they have been explored as an alternative for conventional absorbents for removing $H_2S$ from gas streams and sediments as summarized in **Table 1**. For example, Montes-Morán et al. (2012) exposed < 212 mm and 212-500 mm sized Linz-Donawitz (LD) slag to 1,000 ppmv (1.39 g/m$^3$ at 25 °C and 1 atm) $H_2S$ gas at relative humidity (RH) of 10 and 50% in a fixed bed reactor and observed a maximum $H_2S$ removal of 180 g $H_2S$/kg slag for 212-500 mm sized slag. Kim et al. (2012) and Asaoka et al. (2013) analyzed $H_2S$ removal from the $H_2S$ solution using steel slag by simulating conditions that prevail in pore water of organically enriched sediments. Apart from testing $H_2S$ removal potential of BOF slag in batch reactor (**Table 1**), Sarperi et al. (2014) used BOF slag to treat biogas from anaerobic digester with an aim to upgrade the raw biogas for vehicle fuel use (bio-CNG). The slag showed complete removal of $H_2S$ from raw biogas consisting of 250 ppmv of $H_2S$ in the 2-hour exposure time. Some studies such as Caicedo-Ramrez et al (2020) used basic oxygen furnace (BOF) steel

stag in anaerobic sludge digesters to sequester phosphate and $H_2S$ and achieved 78% removal of $H_2S$ from biogas in 160 days of continuous operation.

Although plenty of information exists on purification of biogas using iron oxides as well as $CO_2$ sequestration with steel slag, little is known about the simultaneous interaction of $CO_2$ and $H_2S$ with the steel slag and the underlying reaction mechanisms. Most of the studies focus on removal of $CO_2$ and $H_2S$ by steel slag independently and none of the studies have explored the potential of BOF slag to remove $CO_2$ and $H_2S$ simultaneously under landfill conditions. The main objectives of this study are to investigate the potential of BOF slag to remove $CO_2$ and $H_2S$ from the LFG and to identify the basic mechanisms responsible for the removal process. In this regard, laboratory batch tests and column tests were conducted to quantify the simultaneous $CO_2$ and $H_2S$ removal capacity of the slag and analyze the effect of various parameters such as moisture content and slag particle size on the $CO_2$ and $H_2S$ removal capacity.

## Materials and Methods

### *Material Preparation and Characterization*

The BOF slag was obtained from Arcelor Mittal Steel Plant, Indiana Harbor East, Indiana, USA. Freshly crushed and dried BOF slag sample was obtained with a top sieve size of 10 mm (3/8 in.) The samples were stored in 5-gallon buckets with airtight lids to prevent carbonation reactions with atmospheric $CO_2$. The specific gravity of the slag was determined as per ASTM D854-14 (2014). The loss-on-ignition (LOI), which typically represents organic content, was determined as per ASTM D2974 (2020) and particle size distribution was evaluated as per ASTM D6913/6913M

142 (2017) and D7928 (2017). The pH and redox (oxidation reduction) potential of the slag was
143 measured using a pH meter (Orion 720A model, Orion Research, Inc. Beverly, Ma, USA) at a
144 liquid to solid ratio of 4:1. Water holding capacity (WHC) of slag was determined by measuring
145 the water retained in the slag after gravity drainage.

146 Three different gradations of BOF slag were used. The BOF slag obtained from the plant
147 in its original particle size distribution was termed as "as-is". BOF slag passing US No. 4 sieve
148 (4.75 mm) and retained on US No. 60 (0.25 mm) was termed as "coarse" and the BOF slag passing
149 US No. 140 sieve (0.106 mm) was termed as "fine" slag. The metal oxides and minerals present
150 in the BOF slag were quantified before and after experimentations using X-ray fluorescence (XRF)
151 and quantitative X-ray powder diffraction (QXRD) with Rietveld quantification analysis using
152 procedures outlined by Reddy et al. (2019a). The morphological changes in the BOF slag were
153 analyzed by scanning electron microscopy (SEM) using a JEOL JSM-6320F High Resolution
154 Scanning Microscope operated at 2.5 kV accelerating voltage and Oxford X-Ray Energy
155 Dispersive Spectrometer (XEDS) fitted with a Hitachi S-3000N Variable Pressure Electron
156 Microscope, respectively.

157

158 ***Batch Experiments***

159

160 Two suites of batch experiments were conducted along with the controls (without slag). Suite I
161 was conducted with the fresh as-is BOF slag at four different moisture contents [MCs; 0, 10, 20,
162 30% by weight (*w/w*)]. The BOF slag (1 g) was placed in a 125 ml glass serum vial (WHEATON®,
163 Millville, NJ, USA) and required amount of deionized water was added to each vial to achieve the
164 target MC. The vial was then purged with synthetic LFG [50% $CO_2$, 48.25% $CH_4$ and 1.75% $H_2S$

(*v/v*)] and hermetically sealed with rubber septa and secured with aluminum crimp cap. The vials were shaken rigorously for approximately 30 seconds to facilitate contact between the slag and the LFG. The headspace gas was analyzed at regular intervals until 24 hours. Suite II was conducted following similar procedure except that the slag was exposed to 20% $H_2S$ (*v/v*) and the MCs tested were 10, 15 and 20% (*w/w*), and the headspace gas was analyzed until the concentration of $H_2S$ became invariant.

For both suites, samples were extracted from the vials with a 1 mL gas tight syringe and were analyzed using SRI 9300 gas chromatography (GC) machine (SRI Instruments, Torrance, CA, USA) equipped with thermal conductivity detector (TCD) for the detection of $CH_4$ and $CO_2$. SRI Model 110 stand-alone detector chassis with electronic pressure control equipped with flame ionization/flame photometric detector (FID/FPD) was connected to the host GC with a heated transfer line for the detection of $H_2S$. HayeSep-D packed column 6' x 1/8'' for separation of $CH_4$ and $CO_2$, and MXT-1 capillary column for separation of $H_2S$ were fitted in the host GC. A T-connection was attached to the inlet port of the host GC for splitting of the gas samples into the two columns. Helium and hydrogen were used as the carrier gases for TCD and FID/FPD, respectively.

***Column Experiments***

Column experiments were conducted to gain insights on the interaction of $CO_2$ and $H_2S$ with the slag under continuous LFG flow condition and the effect of slag particle size on the $CO_2$ and $H_2S$ removal. Experiments were conducted in Chromaflex glass columns (Cole-Parmer, Vernon Hills, Illinois, USA) of 30 cm height and 2.5 cm internal diameter, top and bottom outfitted with bed

support meshes, end connections, and screw caps, as detailed by Reddy et al. (2019a, b). Three BOF slag gradations (as-is, coarse, and fine) at a MC of 10% (*w/w*) were packed using 5 cm lifts and light tamping in each column. Dry synthetic LFG [50% $CO_2$, 48.25% $CH_4$ and 1.75% $H_2S$ (*v/v*)] was injected into each column in an upward flow mode at an inlet pressure of ~10 psi (69 kPa). Dry gas was used to avoid the potential for immediate precipitation of sulfur from interaction of $H_2S$ with water during humidification. The inlet flow rate was controlled by flowmeters (Cole-Parmer, Model No. PMRI-010874). The inlet flowrates of 6-12 ml/min were maintained to ensure the following fluxes; 1) $CH_4$: 5,500-10,500 g $day^{-1}$ $m^{-2}$; 2) $CO_2$: 16,000-30,560 g $day^{-1}$ $m^{-2}$; and 3) $H_2S$: 430-830 g $day^{-1}$ $m^{-2}$. These fluxes used were much higher than the field reported $CH_4$ fluxes ranging from 0.0002 to 4,000 g $day^{-1}$ $m^{-2}$ (De Visscher et al. 1999). The inlet and outlet gas samples were analyzed regularly with the GC. Two sets of column experiments were performed:

1) In the first set, two column tests were performed with as-is BOF slag. One test was terminated just after the breakthrough of $CO_2$ gas, whereas the second when $CO_2$ and $H_2S$ removal capacity was exhausted (e.g. $C_{out}/C_{in}$ of $CO_2$ and $H_2S \cong 1$). The main goal was to quantify the major mineralogical changes associated with short-term and long-term $CO_2$ and $H_2S$ removal.
2) In the second set, three column tests were performed with coarse, as-is and fine BOF slag each. The tests were terminated when the $CO_2$ and $H_2S$ removal capacity was exhausted ($C_{out}/C_{in}$ of $CO_2$ and $H_2S \cong 1$). Here the goal was to investigate the effect of BOF slag particle size on removal capacity and identify the principle reaction mechanisms for the removal of $CO_2$ and $H_2S$ by BOF slag.

XRF and QXRD analyses were conducted on the BOF slag samples at several key intervals of interest to identify the elemental and mineralogical changes in the slag due to reaction with $CO_2$

and $H_2S$. Additionally, SEM-EDS analyses were performed on the slag samples before and after exposure to synthetic LFG and 20% $H_2S$ (*v/v*) to evaluate the morphological changes in the slag.

## Results and Discussion

### *Material Characterization*

Specific gravity and pH of the BOF slag were 3.34 and 12.4, respectively, which are consistent with the previous studies (Reddy et al. 2019c). **Figure 1** shows the particle size distribution of each BOF slag sample. The coarse BOF slag was classified as poorly graded sand (SP) per Unified Soil Classification System (USCS) with mean particle size ($D_{50}$) of 1.8 mm. The as-is BOF slag had fines content of ~ 14%, $D_{50}$ of 0.82 mm, and classified as silty sand (SM). The fine BOF slag had $D_{50}$ of 0.06 mm and classified as low plasticity silt (ML). The LOI/organic content of the slag was low (1.94%) which suggested lack of carbonation for the initial condition. The WHC capacity of the slag was 30% (*w/w*) which is comparable to the landfill cover soils (Reddy et al. 2019a).

**Tables 2, 3** and **4** summarize the elemental composition, bulk chemistry, and mineral phases, respectively, present in the BOF slag as a function of various exposure conditions. The major elements present in the slag are Ca, Fe, Mg, and Si (**Table 2**). The ranges of metal oxides in the original (fresh) BOF slag (**Table 3)** are consistent with the bulk chemistry reported in other studies (Yildrim and Prezzi, 2011; Reddy et al. 2019c; Shi 2004). The original (fresh) BOF slag contained minerals (**Table 4**) known to have high affinity for $CO_2$ and $H_2S$ (Huijgen et al. 2006; Reddy et al. 2019a, b; Ng et al. 2017; Kim et al. 2012; Montes-Morán et al. 2012). Free lime (CaO), portlandite [$Ca(OH)_2$] and larnite ($Ca_2SiO_4$) have the potential to bind $CO_2$ as stable carbonates,

234 as detailed elsewhere (Reddy et al. 2019a, b). The slag contains high amount of $Fe_2O_3$ (29.7%)
235 and FeO (9.6%) which are known to react with $H_2S$ as shown in **Eqs. 2 and 4** (Montes-Morán et
236 al. 2012; Kim et al. 2012; Cantrell et al. 2003; Davydov et al. 1998; Sarperi at al. 2014).
237
238 ***Batch Experiments***
239
240 Batch experiments were performed to analyze the interaction of BOF slag with synthetic LFG
241 components ($CH_4$, $CO_2$ and $H_2S$). There was no noticeable absorption of $CO_2$ at 0% (*w/w*) MC (in
242 dry state) of the BOF slag as shown in **Figure 2**. $CO_2$ removal increased sharply within one hour
243 of exposure to LFG, and the $CO_2$ concentration reduced from 50% (*v/v*) to nearly 15% (*v/v*) leading
244 to 70% removal of $CO_2$ when the moisture was increased from 0 to 10% (*w/w*) (**Figure 2a**).
245 However, the $CO_2$ removal rate did not vary significantly when the moisture was increased from
246 10 to 30% as depicted by the similar slopes of $CO_2$ concentration versus time plot in **Figure 2a**.
247 The $CO_2$ removal capacity of BOF slag reduced gradually after one hour as depicted by the change
248 in slope of $CO_2$ concentration curve from nearly 20 to 2 in the first 3 hours and by 5 hour the slope
249 was essentially asymptotic (**Figure 2a).** An overall $CO_2$ removal of 68-76 g $CO_2$ $kg^{-1}$ BOF slag
250 was obtained which is consistent with the $CO_2$ sequestration capacity reported in Reddy et al.
251 (2019a). Consistent with $CO_2$, there was no $CH_4$ removal in the dry state (0% MC) (**Figure 2b**).
252 Under moist conditions, the slag showed nominal removal of $CH_4$, leading to nearly 20–26%
253 removal or 8–11 g $CH_4$ $kg^{-1}$ BOF slag. Similar to $CO_2$ and $CH_4$, the slag showed no affinity towards
254 $H_2S$ in dry state (**Figure 2c**). However, $H_2S$ removal was significantly affected by moisture leading
255 to 100% removal within 24 hours for all MCs tested (**Figure 2c**). There was no significant impact
256 of presence of $H_2S$ on the $CO_2$ removal capacity or vice versa. **Figure 2d** shows the corresponding

$H_2S$ removal capacity as g $H_2S$ $kg^{-1}$ BOF slag. Since the initial concentration of $H_2S$ in the synthetic LFG was low (~1.75%), a removal of only 2.7 g $H_2S$ $kg^{-1}$ BOF slag was obtained when the amount of $H_2S$ in the batch reactor was completely exhausted.

The $H_2S$ with initial concentration of 1.75% (*v/v*) was rapidly removed, as a result additional series of batch experiments were performed with higher initial $H_2S$ concentration of 20% (*v/v*) at various MCs to evaluate the maximum $H_2S$ removal capacity of the BOF slag (**Figure 3**). **Figure 3a** shows $H_2S$ concentrations as a function of exposure time and initial MC. An increasing $H_2S$ removal was observed with MC. After one hour, the BOF slag with 20% (*w/w*) MC showed more cumulative $H_2S$ removal than at lower MC values (**Figure 3b**), however, the removal capacity dropped off significantly after an hour. After 120 hours, the $H_2S$ removal capacity was nearly saturated (**Figure 3a**) attaining 17.8, 21.7 and 27 g $H_2S$ $kg^{-1}$ BOF slag, respectively as a function of time **(Figure 3b)**.

One of the most important reaction steps for carbonation of steel slag is dissolution of minerals and $CO_2$ gas in the solution resulting in the precipitation of carbonates (Librandi et al 2019; Ukwattage et al. 2017; O'Connor et al. 2001). Hence, moisture plays an important role but increasing the MC above 10% (*w/w*) does not significantly improve/impact the carbonation capacity of the BOF slag. The steep slope of the $CO_2$ removal plot in **Figure 2a** likely corresponds to the free CaO, $Ca(OH)_2$ and $Ca_2SiO_4$ of the slag (**Table 4**, fresh as-is) readily reacting with $CO_2$ as these minerals showed sharp decrease in weight % at $CO_2$ breakthrough (in column tests) which is discussed in detail in the next section. The gradual decrease in the slope of the $CO_2$ removal curve suggests progressive dissolution of the minerals from the inner core of the BOF slag. The BOF slag showed some noticeable removal of $CH_4$ (**Figure 2b**) which could be mere adsorption. **Figure 2c** shows the influence of MC on $H_2S$ removal was stronger than that for $CO_2$ removal.

Sarperi et al. (2014) reported dramatic differences in $H_2S$ removal as a function of moisture, 37 g $H_2S$ $kg^{-1}$ BOF slag at 0% (*w/w*) MC versus 142 g $H_2S$ $kg^{-1}$ BOF slag at 35% (*w/w*) MC. The BOF slag showed significantly higher $H_2S$ removal rates (0.53 g $H_2S$ $hr^{-1}$) at 30% (*w/w*) MC than at lower MCs (0.11–0.13 g $H_2S$ $hr^{-1}$) (**Figure 2d**) which is consistent with the previous findings. The increase in $H_2S$ removal was not very significant when the MC was increased from 10 to 20% (*w/w*), but rapid removal of $H_2S$ occurred when the MC increased from 20 to 30% (*w/w*). The long-term exposure of BOF slag to 20% (*v/v*) $H_2S$ showed an increasing trend in $H_2S$ removal with moisture (**Figure 3**) consistent with the observations of Sarperi et al. (2014) whose $H_2S$ removal was 37, 119 and 142 g $H_2S$ $kg^{-1}$ BOF slag at 0, 20 and 35% (*w/w*) MCs, respectively. Sarperi et al. (2014) reported very high $H_2S$ removal capacity (142 g $H_2S$ $kg^{-1}$ BOF slag) for continuous stirring of batch reactors at 300 rpm. The slag with 20% (*w/w*) MC showed significantly higher $H_2S$ removal (2.5–4 times) in first one hour than that with 10% and 15% (*w/w*) MCs (**Fig. 3b**) which could be attributed to the rapid dissolution of the $H_2S$ in the presence of higher moisture leading to significant sulfur precipitation (**Eq. 1**). Similarly, the high pH of the slag favors the absorption of the $H_2S$ as the pKa for $H_2S/HS^-$ is 7. Moisture also plays an important role in the reductive dissolution of iron oxides by $H_2S$. Ferric oxide ($Fe_2O_3$) precipitates as ferric hydroxide [$Fe(OH)_3$] in solution. Davydov et al. (1998) showed that the amorphous $Fe(OH)_3$ expresses more reactivity with $H_2S$ than the same mass of anhydrous $Fe_2O_3$. **Figure 3a** shows two stage reaction mechanism for the $H_2S$ removal, initial rapid removal with nearly 70–90% of total removal occurring in the first 24 hours which was followed by a relatively slower removal rate (flatter $H_2S$ removal curves after 24 hours). The initial rapid removal could be attributed to the interaction of $H_2S$ with the surficial $Fe(OH)_3$ and formation of elemental sulfur as shown in **Eq. 1**. The second stage with relatively slower $H_2S$ removal rate could be attributed to reductive dissolution of $Fe_2O_3$ lying

303 below the surface layers forming bulk ferric sulfides ($Fe_2S_3$) as shown in **Eq. 2** (Davydov et al.
304 1998).
305
306 ***Column Experiments***
307
308 The first set of column experiments were conducted with as-is BOF slag. One experiment was
309 stopped shortly after breakthrough of $CO_2$ (~100 PV) and another was continually exposed to
310 synthetic LFG until $C_{out}/C_{in}$ of $CO_2$ and $H_2S$ became invariant. **Figure 4** shows the breakthrough
311 curve for as-is BOF slag at short term (breakthrough) and long term ($C_{out}/C_{in}$ of $CO_2$ and $H_2S \cong$
312 1) exposure conditions. The second set of column tests was conducted with coarse and fine BOF
313 slag under similar conditions as the first set and was continued until $C_{out}/C_{in}$ of $CO_2$ and $H_2S$
314 became invariant. **Figures 5a** and **5b** show $CO_2$ and $H_2S$ removal potential of coarse, as-is and
315 fine BOF slag in terms of variation of $C_{out}/C_{in}$ with inflow PV of the synthetic LFG. The
316 breakthrough of $CO_2$ happened at around 40, 80 and 200 PVs for coarse, as-is and fine BOF slags,
317 respectively (**Figure 5a**). Similarly, the breakthrough of $H_2S$ occurred at 100, 200 and 2000 PVs
318 for coarse, as-is and fine BOF slags, respectively (**Figure 5b**).
319 **Figures 6a** and **6b** show cumulative removal of $CO_2$ and $H_2S$, respectively in terms of inflow
320 PVs of synthetic LFG. The $CO_2$ removal capacity of BOF slag was mobilized earlier than the $H_2S$
321 removal capacity which could be attributed to the pH dependency of the carbonation reactions. For
322 example, the pH of the fine slag dropped to 9.88 from the initial pH of 12.3 and since the pKa of
323 $HCO_3^-/CO_3^{2-}$ is 10.3, the reduction in pH below 10.3 would limit the availability of $CO_3^{2-}$ ions for
324 binding Ca ions. On the other hand, pKa of $H_2S/HS^-$ is 7 which shows higher availability of $HS^-$
325 ions in the system leading to continued absorption of $H_2S$. The prolonged absorption of $H_2S$ also

suggests possibility of reaction of $H_2S$ with calcium carbonate ($CaCO_3$) as shown in **Eq. 5** (Lin et al. 1995).

$$CaCO_3 + H_2S \rightarrow CaS + H_2O + CO_2 \quad (5)$$

The $CO_2$ removal capacity of slag exhausted ($C_{out}/C_{in} \sim 1$) at around 1,500 PVs of inflow LFG for all three particle sizes of the BOF slag whereas $H_2S$ removal capacity exhausted at different inflow PVs for different particle sizes of the slag. For example, $C_{out}/C_{in}$ of $H_2S$ reached ~1 at 1,200, 1,800 and 3,600 PVs for coarse, as-is and fine BOF slag, respectively. The fine BOF slag showed highest cumulative $CO_2$ removal (~300 g $CO_2$ $kg^{-1}$ BOF slag) followed by as-is (~120 g $CO_2$ $kg^{-1}$ BOF slag) and coarse (~80 g $CO_2$ $kg^{-1}$ BOF slag) BOF slag which is consistent with the observations of Reddy et al. (2019b). The highest $H_2S$ removal was obtained for fine BOF slag which was ~38 g $H_2S$ $kg^{-1}$ BOF slag (**Figure 6b**). The $H_2S$ removal capacity of as-is and coarse BOF slags was mobilized much earlier than the fine BOF slag resulting in a $H_2S$ removal of ~4 g $H_2S$ $kg^{-1}$ BOF slag and ~2 g $H_2S$ $kg^{-1}$ BOF slag, respectively. $H_2S$ removed at breakthrough by fine BOF slag was 23 g $H_2S$ $kg^{-1}$ BOF slag at 2,000 PVs meaning the slag was able to absorb inflowing $H_2S$ completely until 2,000 PVs of inflow LFG and it accounts for 60% of the total $H_2S$ removed by the fine BOF slag. With this $H_2S$ removal potential, a slag cover of 6 inches thick can sequester $H_2S$ for nearly 8 years under a continuous $H_2S$ flux of 3.6 g $H_2S$ $m^{-2}$ $d^{-2}$ (flux derived from 85 g $CH_4$ $m^{-2}$ $d^{-2}$ reported by Scheutz et al. (2009) assuming 1% $H_2S$ present in the LFG).

The long-term $C_{out}/C_{in}$ plot of $CO_2$ is completely coincident with the short-term plot (breakthrough) (**Figure 4**) which shows complete replication of the experiment and is attributed to the consistency in the dissolution kinetics of the minerals involved in $CO_2$ removal process. The $CO_2$ removal potential of the fine slag was significantly higher than the as-is and coarse BOF slag (**Figure 5a**) which was also established in the study by Reddy et al. (2019b). **Figure 5b** shows a

similar pattern in $H_2S$ removal as $CO_2$ with fine slag having significantly higher $H_2S$ removal potential than coarse and as-is. It is interesting to note that the $H_2S$ removal potential of the BOF slag increased significantly when the particle size changed from as-is to fine whereas, the $H_2S$ removal potential of as-is and coarse BOF slag were not significantly different. It shows that the higher surface area of the slag fines is creating favorable environment for the adsorption of $H_2S$ on the slag surface making it available for further reaction with iron oxides. However, in the study by Montes-Moran et al. (2012), the Linz-Donawitz (LD) slag (also known as BOF slag) showed higher $H_2S$ removal for coarser particle size (212–500 μm) than the finer particle size (< 212 μm) and this behavior was attributed to the higher $Fe_2O_3$ content in the larger particle size fractions. In this study, the high surface area of the fine particles seems to have outweighed the higher $Fe_2O_3$ content in the coarse and as-is BOF slag in the $H_2S$ removal process.

***Mineralogical Changes in Slag Exposed to LFG***

**Tables 2** shows the elemental changes in the as-is (short term and long term) and fine BOF slag exposed to synthetic LFG in column reactor sampled from the bottom portion (close to LFG intet) of the column. The fine slag showed significant increase in the carbon content, followed by as-is (long-term) and as-is (short-term) (**Table 2**). The increase in carbon content in fine slag corresponds to 77.5 g C $kg^{-1}$ BOF slag which is consistent with $CO_2$ removal of the fine slag in column reactor (81.8 g C $kg^{-1}$ BOF slag or 300 g $CO_2$ $kg^{-1}$ BOF slag). Similarly, the increase in sulfur content in fine slag corresponds to 28 g S $kg^{-1}$ BOF slag which is consistent with the $H_2S$ removal estimated from the column reactor (35 g S $kg^{-1}$ BOF slag or 38 g $H_2S$ $kg^{-1}$ BOF slag).

371 Calcium oxide (CaO) was reduced from 38.5 wt% to 36.6 wt% in as-is BOF slag just after
372 breakthrough and 34.9% at the end of the experiment (after complete mobilization of carbonation
373 capacity) (**Table 3**). The CaO content in fine BOF slag after long term exposure to LFG was 31.3%
374 which is significantly lower than the fresh BOF slag (**Table 3**). A significant increase in LOI was
375 also observed in the fine BOF slag which indicates deposition of carbonates formed due to
376 carbonation. There was 40% reduction in the free CaO content at the breakthrough and 43%
377 reduction at the end of the experiment in as-is BOF slag which shows most of the free CaO reacts
378 until breakthrough. The fine BOF slag showed 100% reduction of free CaO content after
379 carbonation (**Table 4**) which was attributed to the higher surface area leading to higher availability
380 of free CaO for reaction with $CO_2$. Apart from free CaO, amount of $Ca(OH)_2$ and $Ca_2SiO_4$ also
381 decreased following carbonation of the slag. $Ca(OH)_2$ showed 60.2% decrease at breakthrough and
382 78.6% at the end of the experiment in as-is BOF slag. It shows that most of the $Ca(OH)_2$ reacted
383 in the initial phase of the reaction (until breakthrough) after which the decrease in $Ca(OH)_2$ was
384 gradual leading to only additional 18.4% reduction in $Ca(OH)_2$ after breakthrough to the
385 termination of the experiment. The fine BOF slag showed a reduction of 81.8% $Ca(OH)_2$ at the
386 end of the experiment which is nearly same as that of as-is BOF slag. The reduced reactivity of
387 $Ca(OH)_2$ after breakthrough could be due to the deposition of calcium carbonate ($CaCO_3$) on the
388 slag surface limiting further interaction of $CO_2$ with the minerals underlying the surface which was
389 confirmed by the presence of formations resembling to $CaCO_3$ crystals in the SEM analysis
390 described in detail in the next section. It is interesting to note that significant amount of $Ca_2SiO_4$
391 reacted in the initial phase of carbonation reaction leading to a reduction of 30.2% at breakthrough
392 in as-is BOF slag. The $Ca_2SiO_4$ was reduced by 37.3% and 80.5% in as-is BOF slag and fine BOF
393 slag, respectively at the end of the experiment. The higher reactivity of $Ca_2SiO_4$ in fine BOF slag

than as-is BOF slag which had relatively higher mean particle size than the fine slag further suggests surface area is a governing factor for the reactivity of the minerals. The significant increase in the calcite ($CaCO_3$) content of the slag confirms the carbonation reactions in the slag. The percentage increase in $CaCO_3$ content was greater than the percentage decrease in the free CaO, $Ca(OH)_2$ and $Ca_2SiO_4$ together which means there were other calcium containing minerals contributing to the carbonation reactions. The total $CaCO_3$ identified by QXRD in the as-is BOF slag at breakthrough, and as-is and fine BOF slag at the end of experiment correspond to 76.8, 111, and 278 g $CaCO_3$ $kg^{-1}$ BOF slag, respectively. Considering only free CaO, $Ca(OH)_2$ and $Ca_2SiO_4$ reacted with $CO_2$, the reduction of their wt% as shown in **Table 4** corresponds to a removal of 47.6, 59.2 and 104.3 g$CO_2$ $kg^{-1}$ BOF slag and formation of 108.2, 134.5 and 237.0 g $CaCO_3$ $kg^{-1}$ BOF slag, respectively as per the reactions shown in **Eqs. 6, 7** and **8**.

$$CaO + CO_2 \rightarrow CaCO_3 \quad (6)$$

$$Ca(OH)_2 + CO_2 \rightarrow CaCO_3 + H_2O \quad (7)$$

$$Ca_2SiO_4 + 2CO_2 \rightarrow 2CaCO_3 + SiO_2 \quad (8)$$

The $CO_2$ removal calculated stoichiometrically from the reduction in the free CaO, $Ca(OH)_2$ and $Ca_2SiO_4$ in the slag is less than the experimentally observed values. The elemental composition of the slag showed significant portion of C in amorphous phase which means some of the carbonates could be in the amorphous phase. It further confirms the hypothesis that there are minerals other than the three above mentioned minerals responsible for carbonation reaction. The other calcium containing mineral which showed decreasing trend was Srebrodolskite ($Ca_2Fe_2O_5$) as shown in **Table 4**. Similarly, the slag had significant amount of Ca in amorphous phase (nearly 35%, **Table 3**) which may also have been responsible for carbonation reactions.

Although the possible reactions of $H_2S$ with steel slag suggest formation of sulfur, FeS and $Fe_2S_3$ (**Eqs. 1, 2 and 4**), no FeS and $Fe_2S_3$ were detected in the QXRD analysis which suggests they could be in the amorphous form (Rickard and Luther 2007). Around 1.15 wt% of crystalline sulfur was detected in the fine BOF slag which corresponds to $H_2S$ removal of 36.6 g $H_2S$ $kg^{-1}$ BOF slag as per the stoichiometric relation shown in **Eq. 1** and is consistent with the $H_2S$ removal capacity quantified from the column experiment (**Figure 6b**). It also confirms that the major reaction mechanism for $H_2S$ removal is precipitation of sulfur. However, it is interesting that no crystalline sulfur was detected in the short term and long term exposed as-is BOF slag samples in the QXRD analysis whereas the elemental analysis shows the presence of sulfur both in crystalline and amorphous phase however, the crystalline phase is significantly lower (**Table 2**). The low crystalline sulfur content in those samples may have resulted in the low intensity peak which appear as a background peak in the search algorithm followed for QXRD thereby preventing the detection of the element.

***Morphological Changes in Slag Exposed to LFG***

**Figure 7** shows the composition based on SEM-EDS analysis of the virgin (fresh) as-is BOF slag, as-is BOF slag exposed to 20% (*v/v*) of $H_2S$ in a batch reactor and coarse, as-is and fine BOF slag exposed to synthetic LFG in column reactor. The values represent average of 3-6 spectra (or locations) on a sample. The QXRD analysis did not show sulfur in coarse and as-is BOF slag exposed to synthetic LFG however, sulfur was detected in the EDS analysis. Although, absolute quantification cannot be done based on the EDS analysis results, it helps to give an idea on the compositional changes occurred on the sample surfaces. The BOF slag exposed to 20% (*v/v*) $H_2S$

showed highest sulfur content which is reasonable as the slag surface was completely free for $H_2S$ absorption without competition for available sites for carbonation.

**Figures 8 (a-h)** show SEM images of virgin as-is BOF slag, coarse, as-is and fine BOF slag exposed to synthetic LFG in column reactor, and as-is BOF slag exposed to 20% (*v/v*) $H_2S$ in a batch reactor. All the SEM micrographs were taken at a scale of 1 μm except for coarse BOF slag which showed significant charging effects at that scale hence the SEM image for coarse BOF slag corresponds to 10 μm scale (**Figure 8b**). It is hard to differentiate between carbonate and sulfur crystals from the SEM micrographs as the samples were exposed to mixture of $CO_2$, $CH_4$ and $H_2S$ in column reactors, however some distinct crystalline features were captured on the slag surfaces which were remarkably different from the carbonate crystal structures. The coarse and as-is BOF slag exposed to synthetic LFG showed rhombohedral crystals (**Figures 8b** and **8c,** respectively) covering the slag surface which can be identified as carbonate crystals based on previous studies (Reddy et al. 2019a, b, c). This further confirms the hypothesis that the formation of $CaCO_3$ on the slag surface could be limiting the interaction of $CO_2$ with the underlying minerals. Sulfur commonly exists in powdery form with fine acicular crystals which are very fragile and have the tendency to break and thus appear like powder (Sarbu et al. 2018). The fine BOF slag exposed to synthetic LFG (**Figure 8e**) and as-is BOF slag exposed to 20% (*v/v*) $H_2S$ (**Figure 8g**) showed powdery appearance covering the rhombohedral and plate like crystals which could be identified as sulfur crystals. Sarbu et al. (2018) reported twinning behavior in sulfur crystals obtained from the sulfur deposits in a sulfur cave. The as-is and fine BOF slag showed some twinning behavior (**Figure 8d** and **8f**, respectively) as observed by Sarbu et al. (2018). However, the twinned crystal structures in fine BOF slag were only observed at higher magnification (100 nm). Unlike slag exposed to synthetic LFG, the slag exposed to 20% (*v/v*) $H_2S$ showed two

462 different shapes of the crystals, fine acicular crystals (**Figure 8g**) which could be sulfur crystals
463 (Xie et al. 2017, Sarbu et al. 2018) and plate like shape (**Figure 8h**) which could be iron sulfides
464 (FeS and $FeS_2$) (Xie et al. 2017; Shimizu et al. 2015). The fact that the slag with 20% (*v/v*) $H_2S$
465 was not exposed to any $CO_2$, there is no possibility for the carbonate crystal formation on the slag
466 surface which further suggests the plate like crystals on the slag surface to be of iron sulfide.
467
468 **Conclusions**
469
470 The study explored the $CO_2$ and $H_2S$ removal potential of BOF slag under LFG conditions by
471 carrying out series of batch and column studies. The study shows the BOF slag can remove $CO_2$
472 and $H_2S$ simultaneously when exposed to synthetic LFG at various moisture conditions. Effect of
473 moisture is more prominent on $H_2S$ removal than on the $CO_2$ removal under similar moisture
474 conditions. Once the slag is in a moist condition, increasing the moisture does not significantly
475 increase the $CO_2$ removal potential whereas, $H_2S$ removal potential of the slag increases
476 significantly with increasing moisture content showing the importance of water of hydration for
477 $H_2S$ dissolution. The particle size of slag affects the $CO_2$ and $H_2S$ removal potential significantly
478 as the slag showed increasing gas removal potential with decreasing particle size which was
479 attributed to the high surface area and greater availability of the minerals for reaction. The
480 mineralogical analysis of virgin BOF slag and BOF slags exposed to LFG under various conditions
481 confirmed that apart from free CaO, $Ca(OH)_2$ and $Ca_2SiO_4$, there are other minerals which may
482 participate in carbonation reactions. The major mechanisms for $H_2S$ removal involved
483 precipitation of sulfur and formation of iron sulfides showing Fe as a responsible element for $H_2S$
484 removal. A maximum $CO_2$ removal of 300 g $CO_2$ $kg^{-1}$ BOF slag and $H_2S$ removal of 38 g $H_2S$ $kg^{-}$

[1] BOF slag was obtained for the BOF slag exposed to synthetic LFG. The assessment of behavior of the BOF slag under real field conditions is underway to further confirm the performance of the BOF slag for simultaneous removal of $CO_2$ and $H_2S$ under landfill conditions.

Using BOF slag in the landfill cover will not only mitigate the harmful emissions like $CO_2$ and $H_2S$, but also provide meaningful use to the steel slags which are otherwise stockpiled or landfilled. Besides, the BOF slag can be used as a filter to purify the LFG for $CH_4$ recovery in the waste to energy plants. The BOF slag, if used in conjunction with biochar amended soil, can mitigate $CH_4$ along with $CO_2$ and $H_2S$ such as in the biogeochemical cover system recently introduced by Reddy et al. (2018). Hence, the future studies need to explore the optimization of the biogeochemical processes and develop a sustainable cover system for the landfills.

## Acknowledgement

This project is funded by the U.S. National Science Foundation (grant CMMI # 1724773), which is gratefully acknowledged. Any opinions, findings, and conclusions or recommendations expressed in this material are those of the authors and do not necessarily reflect the views of the National Science Foundation. Phoenix Services, LLC, is acknowledged for being an industrial partner on this project and providing slag samples for the experiments. Pittsburgh Mineral and Environmental Technology, Inc. and UIC Electron Microscopy Core facility are greatly acknowledged for providing services for sample analysis in this project.

## Data Availability

All data generated during the study appear in this article.

## References


Arkharov, I. A., Simakova, E. N., and Navasardyan, E. S. (2016). Landfill gas as feedstock for energy and industrial processes. *Chem. Pet. Eng.*, 52(7-8), 547-551.

Asaoka, S., Okamura, H., Morisawa, R., Murakami, H., Fukushi, K., Okajima, T., Katayama, M., Inada, Y., Yogi, C. and Ohta, T. (2013). Removal of hydrogen sulfide using carbonated steel slag. *Chem. Eng. J.*, 228, 843-849.

ASTM D854-14 (2014), Standard test methods for specific gravity of soil solids by water pycnometer. ASTM International, West Conshohocken, PA, www.astm.org

ASTM D2974-20e1 (2020). Standard test methods for determining the water (moisture) content, ash content, and organic material of peat and other organic soils. ASTM International, West Conshohocken, PA, 2020, www.astm.org

ASTM D6913 / D6913M-17 (2017). Standard test methods for particle-size distribution (gradation) of soils using sieve analysis. ASTM International, West Conshohocken, PA, 2017, www.astm.org

ASTM D7928-17 (2017). Standard test method for particle-size distribution (gradation) of fine-grained soils using the sedimentation (hydrometer) analysis. ASTM International, West Conshohocken, PA, 2017, www.astm.org

Bergersen, O., and Haarstad, K. (2008). Metal oxides remove hydrogen sulfide from landfill gas produced from waste mixed with plaster board under wet conditions. *J. Air Waste Manage.*, 58(8), 1014-1021.

530 Bonenfant, D., Kharoune, L., Sauve, S., Hausler, R., Niquette, P., Mimeault, M., and Kharoune,
531 M. (2008). $CO_2$ sequestration potential of steel slags at ambient pressure and temperature.
532 *Ind. Eng. Chem. Res*., 47(20), 7610-7616.
533 Caicedo-Ramirez, A., Laroco, N., Bilgin, A. A., Shiokari, S., Grubb, D. G., and Hernandez, M.
534 (2020). Engineered addition of slag fines for the sequestration of phosphate and sulfide
535 during mesophilic anaerobic digestion. *Water Environ. Res.,* 92: 455-464.
536 Chetri, J. K., Reddy, K. R., and Grubb, D. G. (2019). Innovative biogeochemical cover to mitigate
537 landfill gas emissions: Investigation of controlling parameters based on batch and column
538 experiments. *Environ. Process*., 6(4), 935-949.
539 Cantrell, K. J., Yabusaki, S. B., Engelhard, M. H., Mitroshkov, A. V., and Thornton, E. C. (2003).
540 Oxidation of $H_2S$ by iron oxides in unsaturated conditions. *Environ. Sci. Technol.*, 37(10),
541 2192-2199.
542 Davydov, A., Chuang, K. T., and Sanger, A. R. (1998). Mechanism of $H_2S$ oxidation by ferric
543 oxide and hydroxide surfaces. *J. Phys. Chem. B*, 102(24), 4745-4752.
544 Deed, C., Gronow, J., Rosevear, A., et al. (2004). Guidance on gas treatment technologies for
545 landfill gas engines. *Environment Agency*, UK, LFTGN 06.
546 De Visscher, A., Thomas, D., Boeckx, P., and Van Cleemput, O. (1999). Methane oxidation in
547 simulated landfill cover soil environments. *Environ. Sci. Technol.*, 33(11), 1854-1859.
548 He, R., Xia, F. F., Wang, J., Pan, C. L., and Fang, C. R. (2011). Characterization of adsorption
549 removal of hydrogen sulfide by waste biocover soil, an alternative landfill cover. *J. Hazard.*
550 *Mater.,* 186(1), 773-778.
551 Huijgen, W. J., Witkamp, G. J., and Comans, R. N. (2005). Mineral $CO_2$ sequestration by steel
552 slag carbonation. *Environ. Sci. Technol.*, 39(24), 9676-9682.

553 Kim, K., Asaoka, S., Yamamoto, T., Hayakawa, S., Takeda, K., Katayama, M., and Onoue, T.
554 (2012). Mechanisms of hydrogen sulfide removal with steel making slag. *Environ. Sci.*
555 *Technol.*, 46(18), 10169-10174.
556 Ko, J. H., Xu, Q., and Jang, Y. C. (2015). Emissions and control of hydrogen sulfide at landfills:
557 a review. *Crit. Rev. Environ. Sci. Technol.*, 45(19), 2043-2083.
558 Lee, E. H., Moon, K. E., and Cho, K. S. (2017). Long-term performance and bacterial community
559 dynamics in biocovers for mitigating methane and malodorous gases. *J. Biotechnol.*, 242,
560 1-10.
561 Librandi, P., Costa, G., Stendardo, S., and Baciocchi, R. (2019). Carbonation of BOF slag in a
562 rotary kiln reactor in view of the scale-up of the wet route process. *Environ. Prog. Sustain.*
563 *Energy*, 38(3).
564 Lin, S. Y., Al-Shawabkeh, A., Matsuda, H., Hasatani, M., and Horio, M. (1995). $H_2S$ reactions
565 with limestone and calcined limestone. *J. Chem. Eng. Jpn.*, 28(6), 708-714.
566 Montes-Morán, M. A., Concheso, A., Canals-Batlle, C., Aguirre, N. V., Ania, C. O., Martín, M.
567 J., and Masaguer, V. (2012). Linz-Donawitz steel slag for the removal of hydrogen sulfide
568 at room temperature. *Environ. Sci Technol.*, 46(16), 8992-8997.
569 Ng, C. W. W., Xie, M., and Leung, A. K. (2017). Removal of hydrogen sulfide using soil amended
570 with ground granulated blast-furnace slag. *Environ. Eng.*, 143(7), 04017016.
571 O'Connor, W. K., Dahlin, D. C., Nilsen, D. N., Rush, G. E., Walters, R. P., and Turner, P. C.
572 (2001). Carbon dioxide sequestration by direct mineral carbonation: results from recent
573 studies and current status (No. DOE/ARC-2001-029). *Albany Research Center* (ARC),
574 Albany, OR.

575 Occupational Safety and Health Administration, OSHA (2020). U.S. Department of Labor:
576 OSHA: Hydrogen sulfide: Hazards. Available at
577 https://www.osha.gov/SLTC/hydrogensulfide/hazards.html, accessed on March 01, 2020.
578 Petersson, A. (2013). Biogas cleaning. *The biogas handbook*, pp. 329-341. Woodhead Publishing.
579 Reddy, K. R., Grubb, D. G., and Kumar, G., (2018). Innovative biogeochemical soil cover to
580 mitigate landfill gas emissions. Proceedings of the International Conference on Protection
581 and Restoration of the Environment XIV, Thessaloniki.
582 Reddy, K. R., Gopakumar, A., Chetri, J. K., Kumar, G., and Grubb, D. G. (2019a). Sequestration
583 of landfill gas emissions using basic oxygen furnace slag: Effects of moisture content and
584 humid gas flow conditions. *Environ. Eng.*, 145(7), 04019033.
585 Reddy, K. R., Gopakumar, A., Rai, R. K., Kumar, G., Chetri, J. K., and Grubb, D. G. (2019b).
586 Effect of basic oxygen furnace slag particle size on sequestration of carbon dioxide from
587 landfill gas. *Waste Manag. Res.*, 37(5), 469-477.
588 Reddy, K. R., Chetri, J. K., Kumar, G., and Grubb, D. G. (2019c). Effect of basic oxygen furnace
589 slag type on carbon dioxide sequestration from landfill gas emissions. *Waste Manage.*, 85,
590 425-436.
591 Rickard, D., and Luther, G. W. (2007). Chemistry of iron sulfides. *Chem. Rev.*, 107(2), 514-562.
592 Sarbu, S. M., Aerts, J. W., Flot, J. F., Van Spanning, R. J., Baciu, C., Ionescu, A., Kis B. M., Incze,
593 R., Siko-Barabasi, S., Para, Z., Hegyeli, B., Atudorei, N. V., Barr, C., Nealson, K. H.,
594 Forray, F. L., Lascu, C., Fleming, E. J., Bitter, W., and Popa, R. (2018). Sulfur Cave
595 (Romania), an extreme environment with microbial mats in a $CO_2$-$H_2S$/$O_2$ gas chemocline
596 dominated by mycobacteria. *Int. J. Speleol*., 47(2), 7.

597 Sarperi, L., Surbrenat, A., Kerihuel, A., and Chazarenc, F. (2014). The use of an industrial by-
598 product as a sorbent to remove $CO_2$ and $H_2S$ from biogas. *Environ. Chem. Eng.,* 2(2), 1207-
599 1213.
600 Schumacher, M.M. (1983) Landfill methane recovery, Park Ridge, N. J: Noyes Data Corp.
601 Scheutz, C., Kjeldsen, P., Bogner, J. E., De Visscher, A., Gebert, J., Hilger, H. A., Huber-Humer,
602 M., and Spokas, K. (2009). Microbial methane oxidation processes and technologies for
603 mitigation of landfill gas emissions. *Waste Manag. Res.*, 27(5), 409-455.
604 Shi, C. (2004). Steel slag—its production, processing, characteristics, and cementitious properties.
605 *J. Mater. Civil Eng.*, 16(3), 230-236.
606 Shimizu, R., Kubono, I., Kobayashi, Y., and Yamada, Y. (2015). Iron (III) sulfide particles
607 produced by a polyol method. *Hyperfine Interact.*, 231(1-3), 115-121.
608 Spiegel, R. J., Sederquist, R. A., Trocciola, J. C., et al. (1995) Landfill gas treatment system. US
609 Patent 5,451,249, filed Jun. 14, 1994 and issued Sept. 19, 1995.
610 Yildirim, I. Z., and Prezzi, M. (2011). Chemical, mineralogical, and morphological properties of
611 steel slag. *Adv. Civil Eng.*, 2011, 463638.
612 Yildirim, I. Z., and Prezzi, M. (2015). Geotechnical properties of fresh and aged basic oxygen
613 furnace steel slag. *J. Mater. Civ. Eng.*, 27(12), 04015046.
614 Ukwattage, N. L., Ranjith, P. G., and Li, X. (2017). Steel-making slag for mineral sequestration
615 of carbon dioxide by accelerated carbonation. *Measurement*, 97, 15-22.
616 United States Environmental Protection Agency, USEPA. (2020). Landfill methane outreach
617 program (LMOP): Basic information about landfill gas. Available at
618 https://www.epa.gov/lmop/basic-information-about-landfill-gas (accessed on March 31,
619 2020)

620 Więckowska, J. (1995). Catalytic and adsorptive desulphurization of gases. *Catal. Today*, 24(4),
621 405-465.
622 Xie, M., Leung, A. K., and Ng, C. W. W. (2017). Mechanisms of hydrogen sulfide removal by
623 ground granulated blast furnace slag amended soil. *Chemosphere,* 175, 425-430.

**Table 1.** Summary of studies exploring use of steel slag to sequester $H_2S$ under various conditions

| Material | Experimental Condition | Slag Particle Size | Max. $H_2S$ removal | Reference |
|---|---|---|---|---|
| Linz-Donawitz Steel Slag | Reactor: fixed bed quartz reactor<br>Gas condition: 1000 ppmv (1.39 mg $H_2S$/L) $H_2S$ in moist air (RH: 10 and 50%)<br>Temperature: Room temperature (25 ± 2 °C) | < 212 mm; 212-500 mm | 180 g $H_2S$/kg slag | Montes-Morán et al. (2012) |
| Steel making slag (slag type not mentioned | Reactor: 150 mL vial bottle, agitated at 60 rpm<br>Gas condition: $H_2S$ solution with a concentration ranging from 0 to 200 mg S/L<br>Temperature: 25 °C | 2-5 mm | 37.5 g S/kg slag | Kim et al. (2012) |
| Steel making slag-carbonated) (slag type not mentioned) | Reactor: 100 mL vial bottle, agitated at 100 rpm<br>Gas condition: $H_2S$ solution with a concentration of 10 to 100 mg/L<br>Temperature: 25 °C | 0.8-5 mm | 7.5 g $H_2S$/kg slag | Asaoka et al. (2013) |
| BOF slag | Reactor: Batch reactor, agitated at 300 rpm<br>Gas condition: 20 % (v/v) $H_2S$<br>Moisture condition: 0, 20% and 40% (w/w)<br>Temperature: Room temperature (20 °C) | <1 mm, 1-6 mm | 119 g $H_2S$/ kg slag | Sarperi et al. (2014) |
| BOF Slag | Reactor: Anaerobic digestor, slag added at dosages of 1 g/L to 50 g/L<br>Gas condition: Digestor biogas<br>Temperature: 32 ± 2 °C | <1.6 mm | 78% $H_2S$ removal | Caicedo-Ramrez et al. (2020) |
| BOF slag | Reactor: Batch reactor (manual stirring) and fixed column reactor,<br>Gas condition: Synthetic LFG (50% $CO_2$, 48.25% $CH_4$ and 1.75% $H_2S$); 20 % $H_2S$<br>Moisture condition: 0, 10%, 20% and 30% (w/w)<br>Temperature: Room temperature (25 °C) | <0.075 mm, <0.075-4.75 mm, 0.425-4.75 mm | 38 g $H_2S$/kg slag | Current study |

**Table 2**. Normalized elemental composition (wt%) of as-is and fine BOF slags

| Element | Fresh As-is | | Breakthrough As-is (PV = 100) | | Long term exposed As-is (PV = 1,900) | | Long term exposed Fines (PV 4,950) | |
|---|---|---|---|---|---|---|---|---|
| Ca | 43.3 | (A 37.3%) (C 62.7%) | 42.2 | (A 41.8%) (C 58.2%) | 41 | (A 36.7%) (C 63.3%) | 41.8 | (A 26.5%) (C 73.4%) |
| C | 0.8 | (A 71.8%) (C 28.2 %) | 2.6 | (A 39.1%) (C 60.9 %) | 4 | (A 34.9%) (C 65.1%) | 8.55 | (A 10.7%) (C 89.3%) |
| S | 0.1 | (A 77.2%) (C 22.8%) | 0.4 | (A 80.2%) (C 19.8%) | 1.1 | (A 91.5%) (C 8.5%) | 2.9 | (A 0%) (C 100%) |
| Fe | 32.7 | | 32.1 | | 31.9 | | 25.15 | |
| Mg | 10.2 | | 10.1 | | 9.7 | | 10 | |
| Si | 7 | | 7.2 | | 7.5 | | 8.6 | |
| Mn | 2.6 | | 2.6 | | 2.6 | | 2.45 | |
| Al | 1.2 | | 1.2 | | 1.2 | | 1.1 | |
| Ti | 0.4 | | 0.4 | | 0.4 | | 0.4 | |
| P | 0.3 | | 0.3 | | 0.3 | | 0.3 | |
| Cl | 0.1 | | 0.1 | | 0.1 | | 0.2 | |
| V | 0.1 | | 0.1 | | 0.1 | | 0.1 | |
| Na | 0.1 | | 0.1 | | 0.1 | | 0 | |
| H | 0.3 | | 0 | | 0 | | 0 | |
| F | 0 | | 0 | | 0 | | 0 | |
| Zr | 0 | | 0 | | 0 | | 0 | |

**Note:** PV = pore volume; A = amorphous fraction; C = crystalline fraction

**Table 3.** Major oxide chemistry of as-is and fine BOF slags

| Major oxides | Fresh | Breakthrough As-is (PV = 100) | Long-term As-is (PV = 1,900) | Long-term Fines (PV 4,950) |
|---|---|---|---|---|
| CaO | 38.5 | 36.6 | 34.9 | 31.3 |
| $SiO_2$ | 10.4 | 9.9 | 9.4 | 7.95 |
| $Al_2O_3$ | 1.5 | 1.4 | 1.4 | 1.1 |
| $Fe_2O_3$ | 29.7 | 28.4 | 27.7 | 19.25 |
| MgO | 10.7 | 10.4 | 9.8 | 8.9 |
| $SO_3$ | 0.2 | 0.6 | 1.7 | - |
| LOI | 4.8 | 8.8 | 11.4 | 24.5 |

**Note:** PV = pore volume

**Table 4.** Mineralogical evolution of the as-is and fine BOF slags

| Mineral | Formula | Fresh As-is | Breakthrough As-is (PV = 100) | Long-term As-is (PV = 1,900) | Long-term Fines (PV 4,950) |
|---|---|---|---|---|---|
| Amorphous | | 30.7 | 30.3 | 33 | 40.6 |
| Srebrodolskite | $Ca_2Fe_2O_5$ | 17.41 | 15.62 | 14.3 | 7.3 |
| Larnite | $Ca_2SiO_4$ | 16.44 | 11.47 | 10.3 | 3.2 |
| Iron Magnesium Oxide | (MgO)0.593 (FeO)0.407 | 9.58 | 16.09 | 9.3 | 6.5 |
| Wuestite | FeO | 9.19 | 6.66 | 8.4 | 3.15 |
| Magnesioferrite | $MgFe_2O_4$ | 7.79 | 7.57 | 8.6 | 6.5 |
| Lime | CaO | 1.76 | 1.06 | 1 | 0 |
| Portlandite | $Ca(OH)_2$ | 4.67 | 1.86 | 1 | 0.85 |
| Calcite | $CaCO_3$ | 0.43 | 6.19 | 9.6 | 27.8 |
| Vaterite | $CaCO_3$ | 0.75 | 1.49 | 1.5 | - |
| Dolomite | $CaMg(CO_3)_2$ | - | - | - | 1.7 |
| Sulfur | S | - | - | - | 1.15 |

**Note:** PV = pore volume

**Figure Captions**

**Figure 1.** Particle size distribution of the virgin BOF slags: coarse (#4-#60); as-is (original gradation); and fine (passing #140).

**Figure 2.** Simultaneous removal of synthetic LFG components by the as-is BOF slag at 0, 10, 20 and 30% (*w/w*) moisture contents: (a) $CO_2$; (b) $CH_4$ (b); and (c and d) $H_2S$. Solid lines denote gas concentration and dotted lines represent gas removal. Gas concentration 1% (*v/v*) = 10,000 ppmv

**Figure 3.** Removal of $H_2S$ by BOF slag in long term at different moisture contents: (a) variation of concentration and percentage removal with time; (b) cumulative removal at different points of time. Gas concentration 1% (*v/v*) = 10,000 ppmv

**Figure 4.** $CO_2$ removal by BOF slag in short-term (until breakthrough) and in long-term both at 10% (*w/w*) initial moisture content and continuous flow of synthetic LFG (48.25% $CH_4$, 50% $CO_2$ and 1.75% $H_2S$).

**Figure 5.** (a) $CO_2$ and (b) $H_2S$ gas removal in terms of ratio of outlet and inlet gas concentrations as a function of particle size of BOF slag for an initial moisture content of 10% (*w/w*) and continuous flow of synthetic LFG (48.25% $CH_4$, 50% $CO_2$ and 1.75% $H_2S$).

**Figure 6.** (a) Cumulative $CO_2$ and (b) $H_2S$ gas removal as a function of particle size of BOF slag for an initial moisture content of 10% (*w/w*) and continuous flow of synthetic LFG (48.25% $CH_4$, 50% $CO_2$ and 1.75% $H_2S$).

**Figure 7.** SEM-EDS based elemental composition of the various BOF slags including exposed to 20% (*v/v*) $H_2S$ in a batch reactor and synthetic LFG (48.25% $CH_4$, 50% $CO_2$, and 1.75% $H_2S$) in column reactors based on SEM-EDS analysis.

**Figure 8.** SEM images of (a) virgin BOF slag; (b) coarse BOF slag exposed to synthetic LFG in a column reactor; (c and d) as-is BOF slag exposed to synthetic LFG in a column reactor; (e and f) fine BOF slag exposed to synthetic LFG in a column reactor; (g and h) as-is BOF slag exposed to 20% (*v/v*) $H_2S$ in a batch reactor.

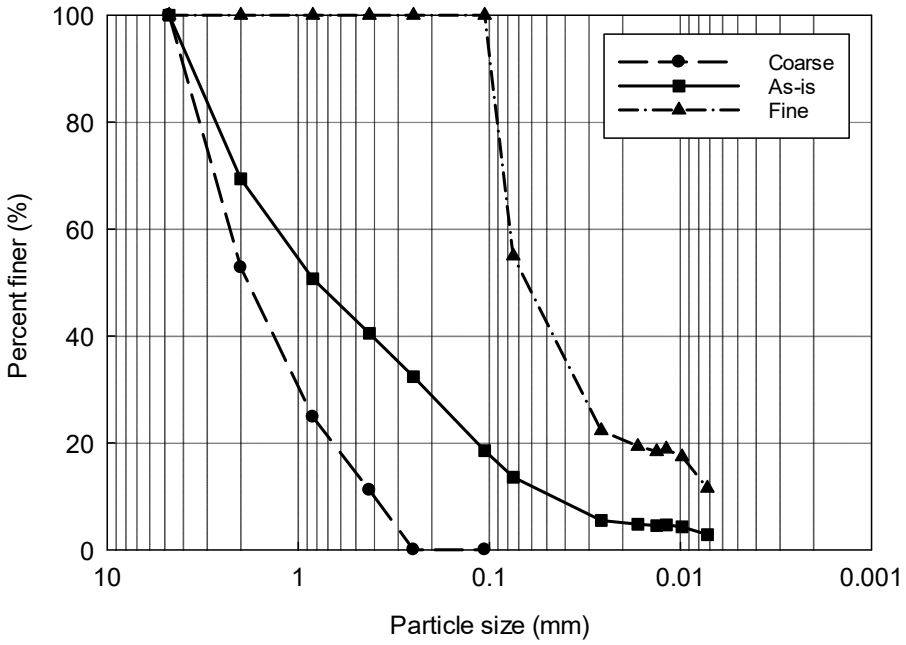
100
80
60
40
20
0
Percent finer (%)
10
1
0.1
0.01
0.001
Particle size (mm)
Coarse
As-is
Fine

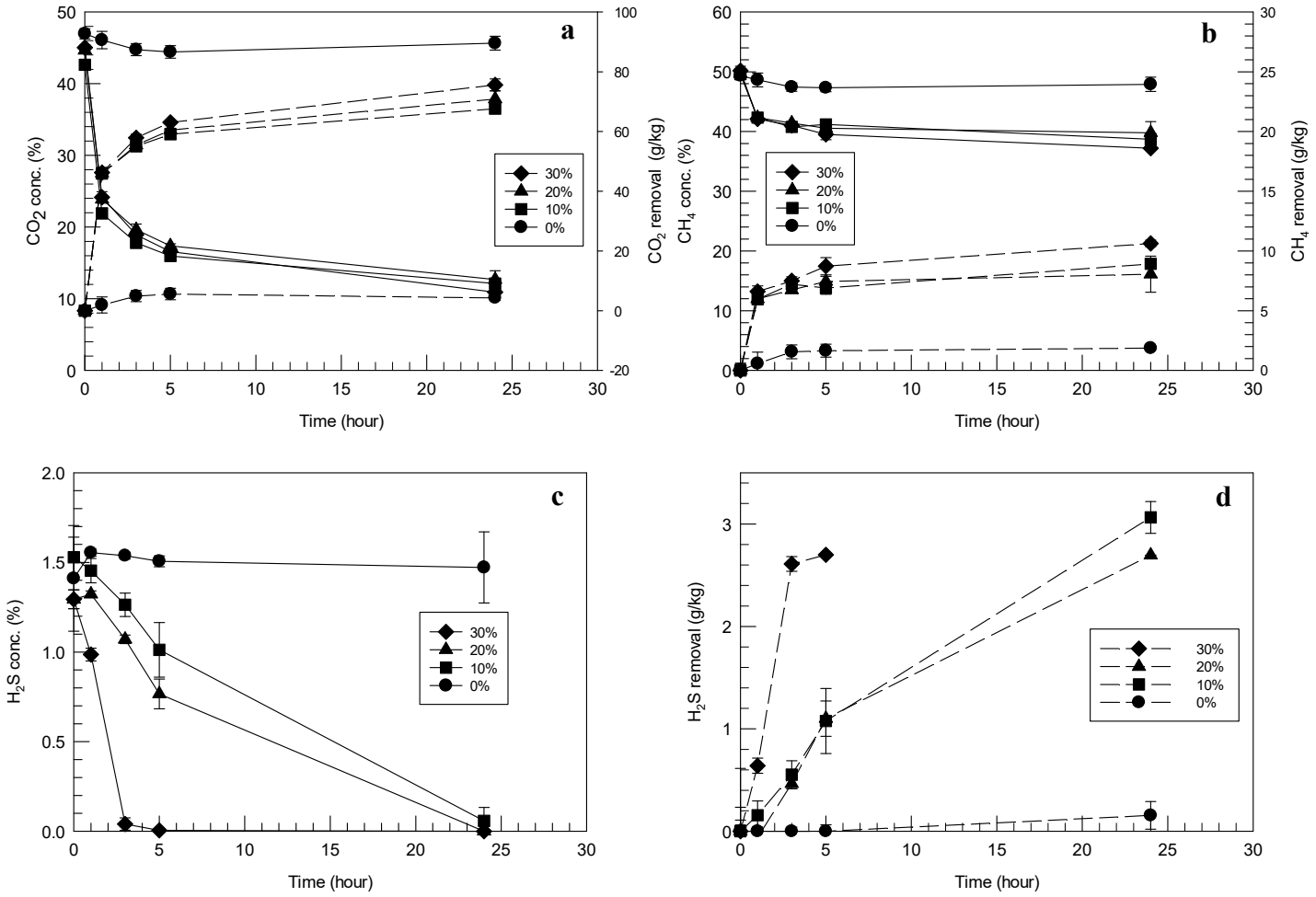
a
$CO_2$ conc. (%)
$CO_2$ removal (g/kg)
Time (hour)
30%
20%
10%
0%
b
$CH_4$ conc. (%)
$CH_4$ removal (g/kg)
Time (hour)
30%
20%
10%
0%
c
$H_2S$ conc. (%)
Time (hour)
30%
20%
10%
0%
d
$H_2S$ removal (g/kg)
Time (hour)
30%
20%
10%
0%

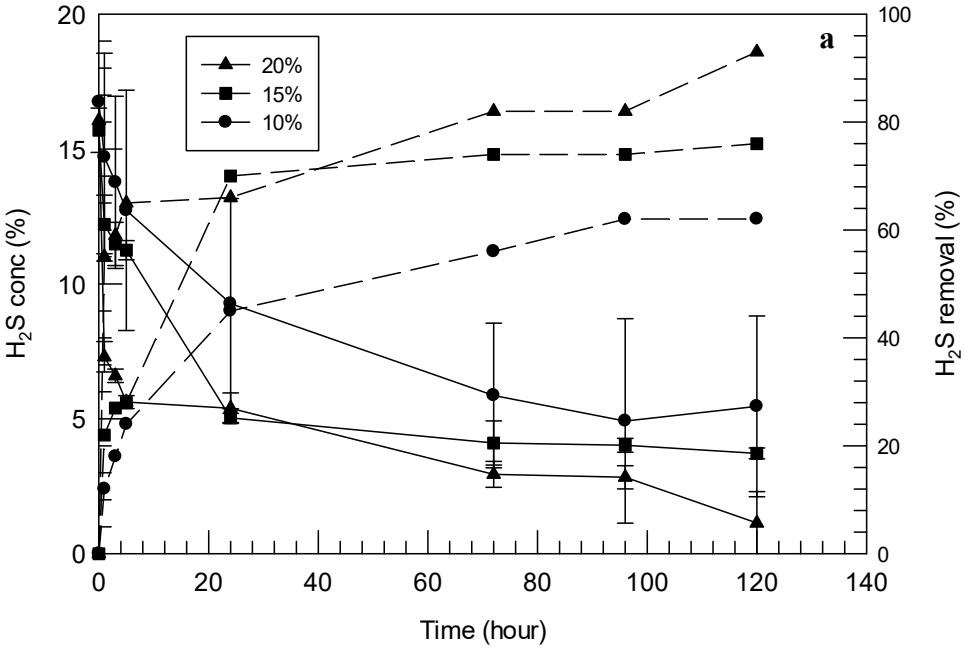
a
20%
15%
10%
H2S conc (%)
H2S removal (%)
Time (hour)
0
5
10
15
20
0
20
40
60
80
100
120
140

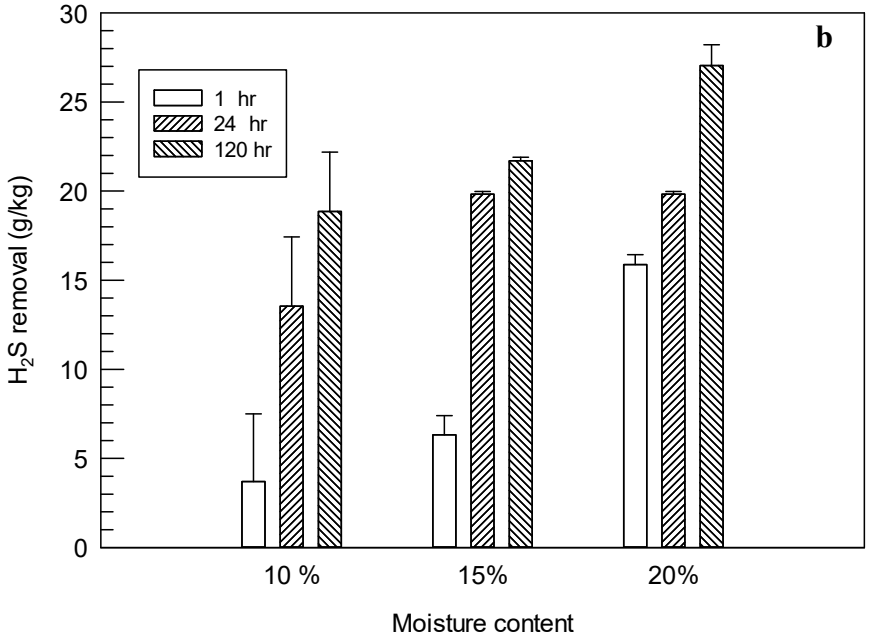
b
1 hr
24 hr
120 hr
H2S removal (g/kg)
10 %
15%
20%
Moisture content
0
5
10
15
20
25
30

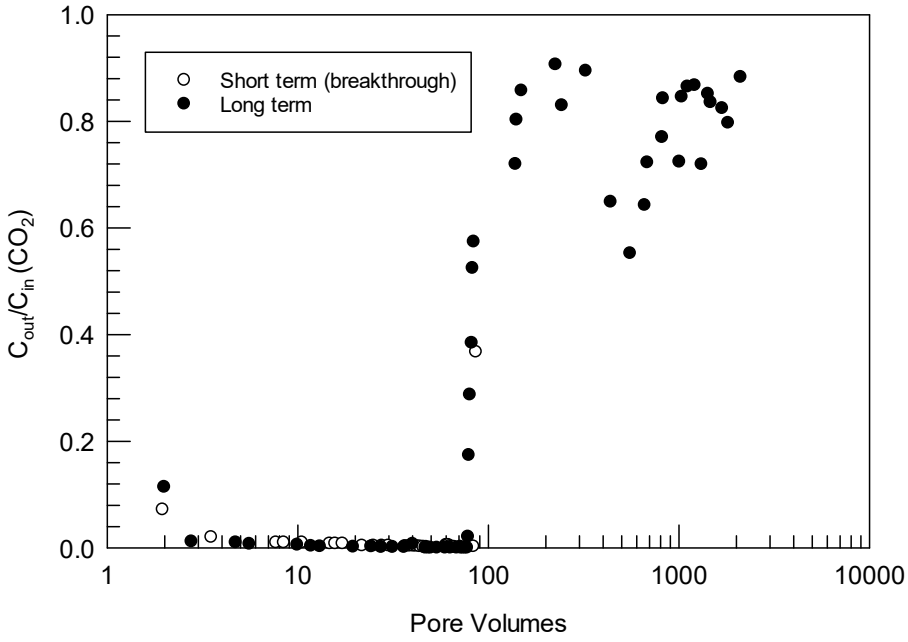
Short term (breakthrough)
Long term
$C_{out}/C_{in}$ ($CO_2$)
Pore Volumes
0.0
0.2
0.4
0.6
0.8
1.0
1
10
100
1000
10000

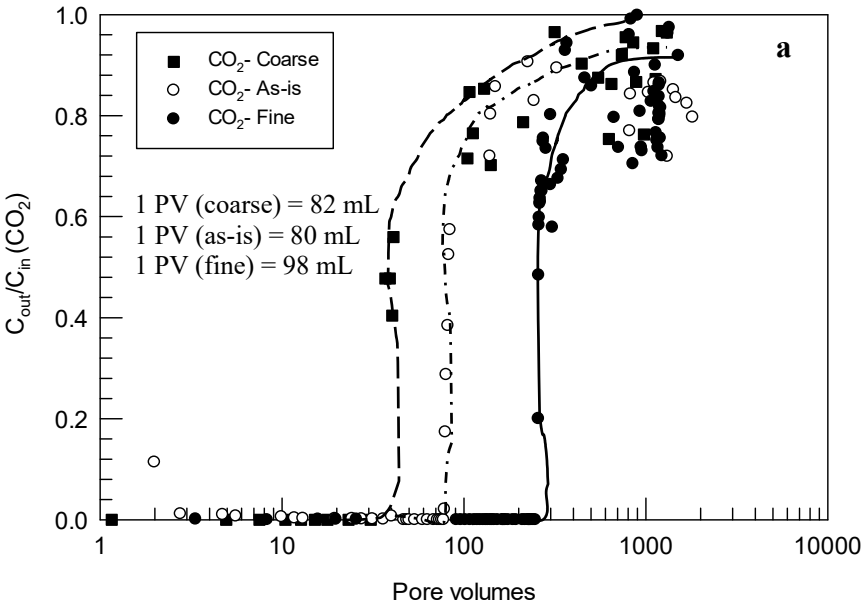
a
CO2- Coarse
CO2- As-is
CO2- Fine
1 PV (coarse) = 82 mL
1 PV (as-is) = 80 mL
1 PV (fine) = 98 mL
Cout/Cin (CO2)
Pore volumes
1.0
0.8
0.6
0.4
0.2
0.0
1
10
100
1000
10000

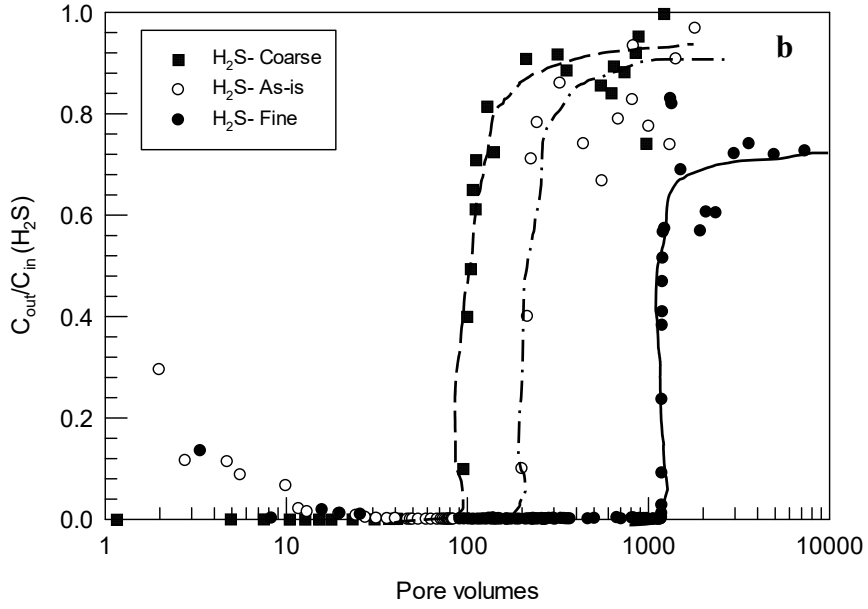
b
H2S- Coarse
H2S- As-is
H2S- Fine
Cout/Cin (H2S)
Pore volumes
1.0
0.8
0.6
0.4
0.2
0.0
1
10
100
1000
10000

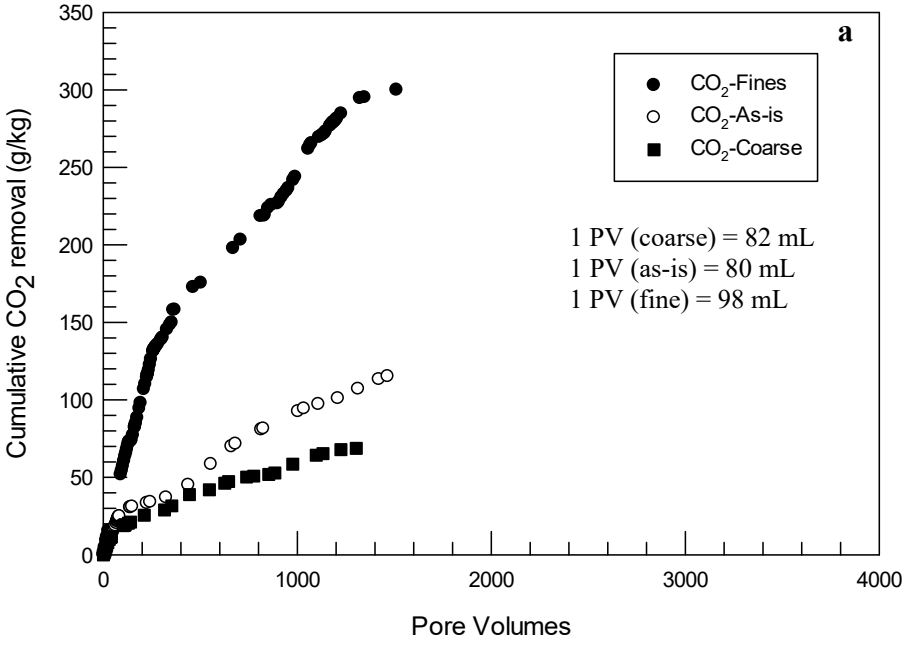
a
CO2-Fines
CO2-As-is
CO2-Coarse
1 PV (coarse) = 82 mL
1 PV (as-is) = 80 mL
1 PV (fine) = 98 mL
Cumulative CO2 removal (g/kg)
Pore Volumes
0
50
100
150
200
250
300
350
0
1000
2000
3000
4000

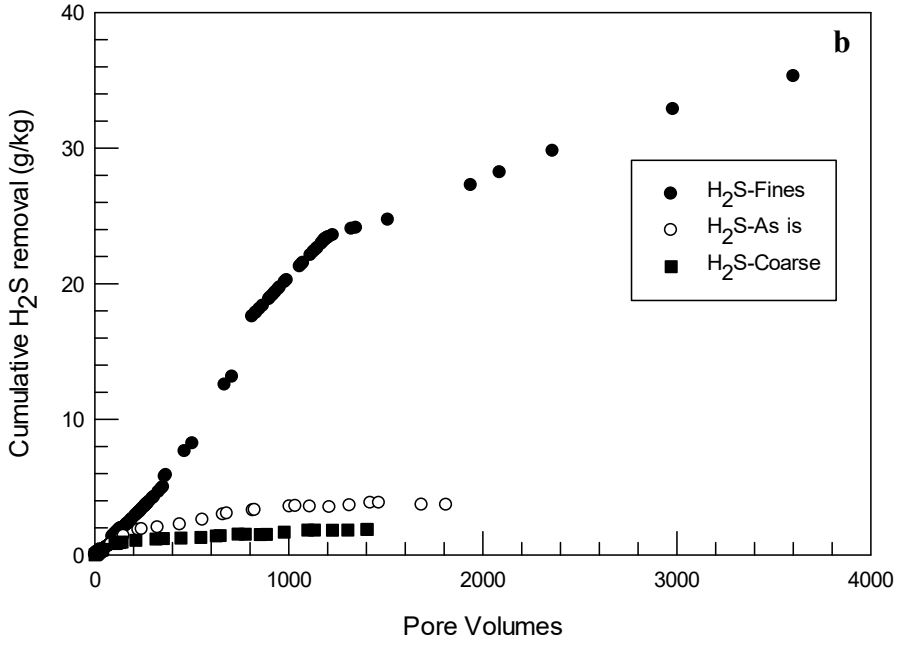
b
H2S-Fines
H2S-As is
H2S-Coarse
Cumulative H2S removal (g/kg)
Pore Volumes
0
10
20
30
40
0
1000
2000
3000
4000

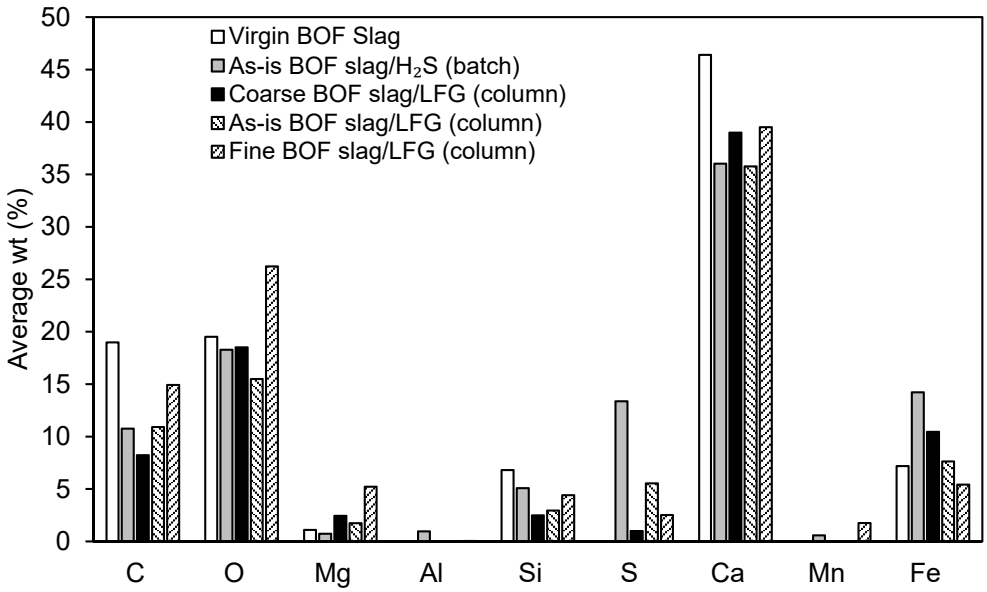
Virgin BOF Slag
As-is BOF slag/H2S (batch)
Coarse BOF slag/LFG (column)
As-is BOF slag/LFG (column)
Fine BOF slag/LFG (column)
Average wt (%)
50
45
40
35
30
25
20
15
10
5
0
C
O
Mg
Al
Si
S
Ca
Mn
Fe

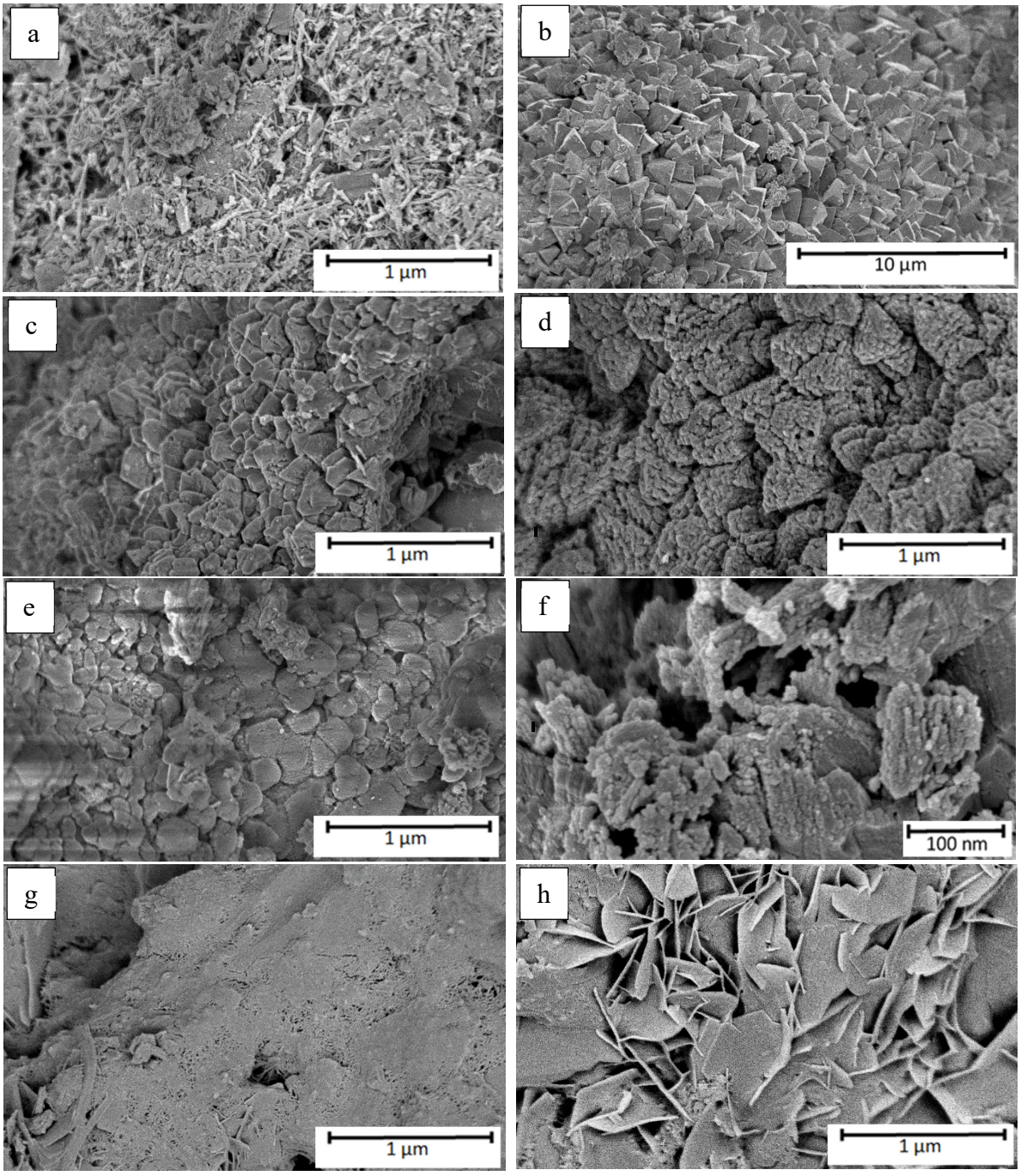
a
1 µm
b
10 µm
c
1 µm
d
1 µm
e
1 µm
f
100 nm
g
1 µm
h
1 µm